ICAS 2021 SHANG HAI
International Council of the Aeronautical Sciences
32nd Congress of the International Council of the Aeronautical Sciences
September 6-10, 2021 Pudong Shangri-La, Shanghai, China

THE AERODYNAMIC OPTIMIZATION AND TRIM CHARACTERISTICS RESEARCH ON VARIABLE CAMBER WING OF WIDE-BODY CIVIL TRANSPORT

Hao Xuan[1], Su Cheng[1], Wang Bin[1], Zhang Qingqing[1]

[1] China Academy of Aerospace Aerodynamics, 17 Yungang West Road, Beijing, 100074, P. R. China

Abstract

The variable camber wing concept is an effective way to improve the load distribution along the wing and has been applied to the aircraft for many years. To research the drag reduction potentiality of variable camber wing technology of wide-body civil transport, the deflection of flaps and ailerons were optimized based on Genetic algorithm. The accurate response surface models based on high fidelity CFD results are developed to realize the fast prediction of aerodynamic characteristics. The amount of 1-5 Counts reduction of the drag coefficient can be obtained for wing-body with nacelle configurations at different flight conditions. The trim characteristics of the optimized configurations were analyzed. For the configurations that generate nose-down moment, the upward deflecting of the inner flap weakens the downwash of the wake to the horizontal tail and the trim ability of the tail is worsened, which results in more trim penalty of drag.

Keywords: variable camber wing, trim characteristics, wide-body transport, optimization

1. Introduction

The high efficiency and low cost characteristics of the commercial transport mainly depend on the engine performance and aerodynamic characteristics. According to Breguet's range formula, the high cruise factor is an important target for aerodynamic design. For traditional civil transport, the final configuration is a compromised configuration with a multitude of design considerations. Additionally, the final design provides nearly-optimal performance for specifically defined flight profiles and results in the aircraft flying at its best-designed performance condition very seldom or only by chance. During the cruise flight, additional configuration changes are unavailable to optimize performance for the vast range of constraints and divergent flight mission.

The variable camber wing concept was firstly practiced by Wright Brothers to make lateral control. Since then, this concept was developed and applied to military aircraft successfully to enhance the maneuver performance and load controlling. The first significant application of variable camber wing to the civil transport was made by Lockheed on the L-1011 aircraft in the early 1970's [1-2]. The Boeing and Airbus evaluated the variable camber wing since 1980's [3-7], and the technique has been applied to the new generation of wide-body civil transport, B787 and A350. For B787, the predicted 0.4 Count in drag reduction can bring a 450kg-reduction for gross weight.

Unlike the military aircraft, this new technology should to be employed at low cost with high reliability once applying to civil transport, thus for B787 and A350, the camber of wings are varied only by deflecting the trailing edge flaps, spoilers and ailerons. The deflecting of flaps and spoilers at inner wing will change the downwash of wake near the area of the horizontal tail[6], thus the trim performance of horizontal tail will be changed by different camber settings. Therefore, for variable camber wing design, people should not only restrict the pitch moment of the basic wing, but also pay attention to the downwash influence on horizontal tail to obtain a proper penalty of trimmed drag.

In this paper, the drag reduction potentiality of variable camber wing technology of wide-body civil transport is optimized based on surrogate model and the trimmed aerodynamic characteristics of the configurations with different camber settings at cruise flight are researched by numerical simulation. In the second section, the methods used in this study are introduced, including the computational fluid dynamics(CFD), the surrogate model, and the genetic algorithm. In the third section, the main results of the optimization are discussed. The conclusions and recommendations for future work are given in the last part of the paper.

2. Methodology

2.1 Model

The half model of wing-body configuration with nacelle (WBN) shown in Figure 1(a) is the research object in this paper. The Mach number(Ma) and coefficient of lift(C_L) at cruise design point for the WBN are Ma=0.85, C_L=0.51, while the basic wing is a compromised solution with the consideration of another two design points, C_L=0.51 at the Mach number 0.83and 0.87 separately to meet the requirement of drag divergent characteristics. The half model of wing-body configuration with nacelle and tails(WBNT) is shown in Figure 1(b), and the cruise point in trimmed condition is Ma=0.85, C_L=0.48. The camber of the wing is altered at trailing edge through the deflecting of inner flap, outer flap and two ailerons, as well as the spoilers, shown in Figure 1(c). The deflection angle of flaps and ailerons are the design variables for camber optimization. The deflections of the spoilers are dominated by flaps deflecting, which are not necessary to be optimized.

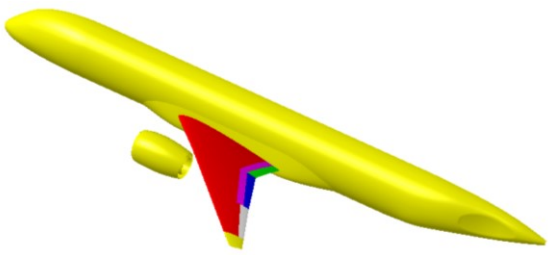

(a) WBN configuration

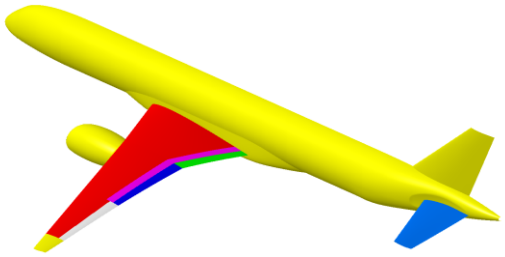

(b) WBNT configuration

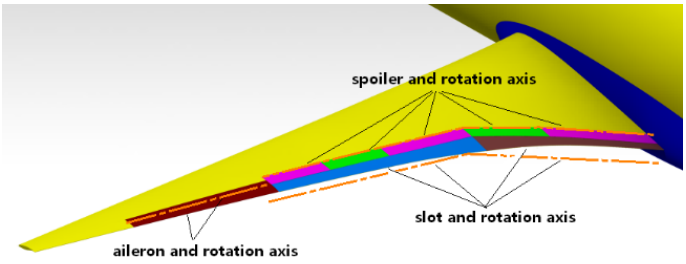

(c) Flaps, aileron and spoilers

Figure 1 Sketch of variable camber wing

2.2 Numerical Simulation

The aerodynamic characteristics were obtained by solving the structured-grid, cell-centered Reynolds-averaged Navier-Stokes (RANS) equation. The third-order upwind-biased spatial differential scheme is chosen for solving the convective and pressure terms, and second-order differential scheme is used to solve the viscous terms. Roe's flux difference-splitting method[8] is used to obtain fluxes at the cell faces. the Menter's k-ω SST turbulence model[9] is used for this study. The solution is advanced in time with an implicit approximate factorization method. The code employs local time-step scaling, grid sequencing and multi-grid to accelerate convergence to steady state.

At the inflow and outflow boundary, the free stream boundary condition with the flow absolute pressure, static temperature, Mach number, and velocity direction are specified. The isothermal no-slip condition is applied at the solid wall.

The point-to-point structured grids are generated and the height of the first layer along the model surface is 5×10^{-6} to ensure the value of y plus to be about 1.0. The total number of grid points is about 14 million. The high fidelity of the code and grid has been validated by a lot of similar models which can be referred in [10][11].

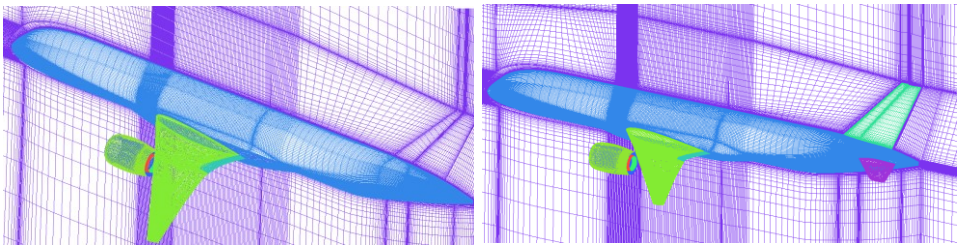

(a) wing body with nacelle (b) wing body with nacelle and tails

Figure 2 Sketch of the computational grid

2.3 Response Surface Model(RSM)

The response surface model[13] developed in the 1950's is a collection of statistical and mathematical techniques useful for developing, improving and optimizing processes in which a response of interest is influenced by several variables and the objective is to optimize this response. The cubic polynomial are used to build the drag and pitch moment prediction model based on CFD simulation results. All databases of candidate designs are obtained by populating the design space using an optimal Latin hypercube sampling technique[14].

2.4 Genetic Algorithm

The genetic algorithm (GA)[12] is used in the optimization. The GA is based on Darwin's "survival of the fittest" evolutionary concept. It employs selection, crossover and mutation operators to "evolve" a population of individual designs over many generations. The genetic algorithm has the ability to deal with a large number of continuous and integer design variables and locate the global optimum without an initial design point, which brings the successful application in engineering design and optimization problems.

The fitness of each design is determined based on its performance, which is evaluated by the RSM based on the high fidelity CFD data in this paper. GA operators are used to create the next generation. Applying the "survival of the fittest" rule, only the individuals that possess promising fitness are allowed to reproduce or pass directly to the next generations. The process continues until a certain convergence criterion is reached.

3. Results

3.1 RSM Model Validation

Since the amount of drag reduction is very tiny, the accuracy of the surrogate model will have a significant influence on the validity of the optimization results for variable camber wing. In this section, the required number of sample points to ensure a reliable RSM model was researched by multi-step optimization.

First of all, 40 sample points were generated by Optimal Latin hypercube method for 4 design variables. The range of deflection angle of inner and outer flap are [-1°, 1°] and [-1°, 2°], separately. The deflection angle range of inner and outer ailerons are all from -1° to 3°. The downward deflecting is prescribed positive for both the flaps and ailerons. The coefficients of drag(C_D) and pitch moment(C_M, positive for nose-up) of WBN configurations, were calculated by CFD. The RSM model of the increment of drag(dC_D) and pitch moment(C_M) compared with the basic fixed camber configuration, were built by cubic polynomials. The first step optimization was carried out based on the RSM model built by 40 sample points (40 SPs). Then some preferable optimized results were validated by CFD to verify the precision of RSM model. Combined with the CFD data of optimized results, a new RSM models with 57 sample points (57 SPs) were built. Based on the

new RSM model, the second step optimization was done and another RSM model with 70 sample points (70 SPs) was built followed the above mentioned method. Figure 3-Figure 5 shows the drag and pitch moment results predicted by CFD and the RSM models of 40 SPs, 57 SPs and70 SPs.

It can be seen from Figure 3 that the 40 SPs RSM model can provide an accurate prediction of the sample points (No.1-40 points). Although there exit some discrepancy between RSM model results and CFD results of the optimization points (No. 41-70), especially for the drag with the maximum error of 10%, the 40 SPs RSM model still can provide the correct trend of C_D and C_M varying with the camber. With the sample data refined, both the drag and pitch moment results predicted by 57 SPs' RSM model agree pretty well with the CFD results (Figure 4).

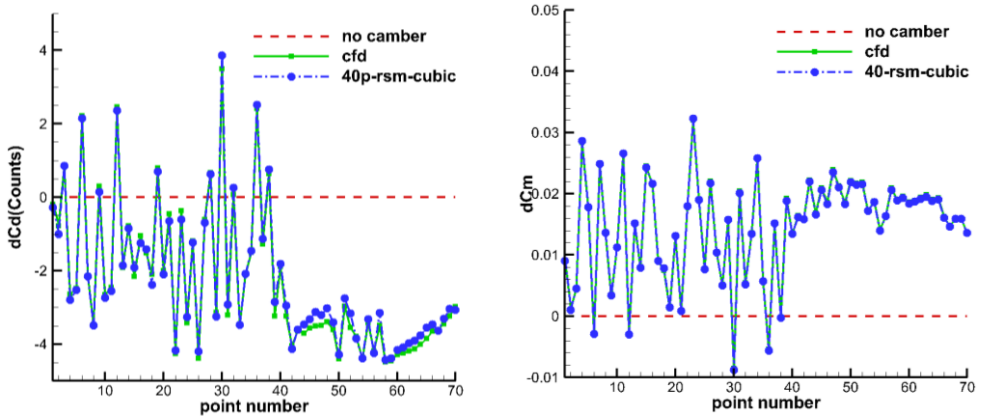

(a) Drag increment (b) Pitch moment

Figure 3 Comparison between 40SPs model and CFD results

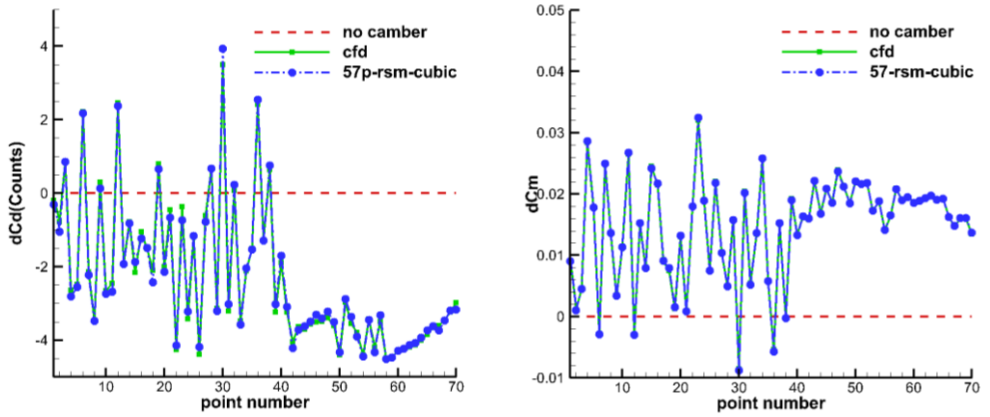

(a) Drag increment (b) Pitch moment

Figure 4 Comparison between 57 SPs model and CFD results

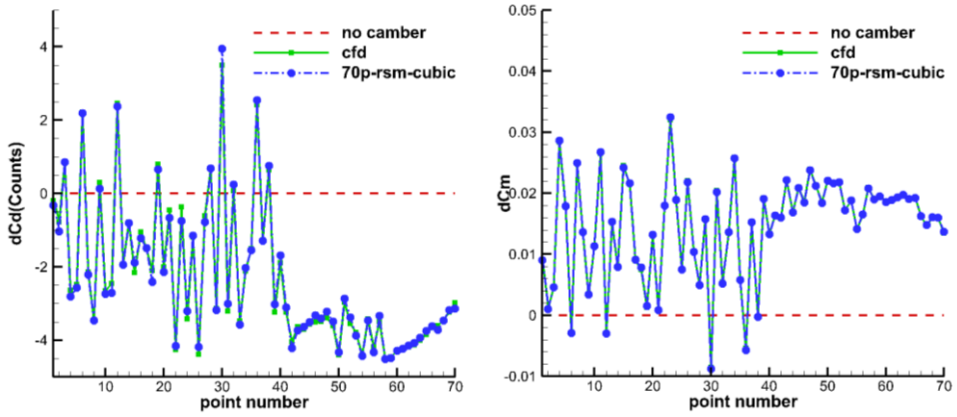

(a) Drag increment (b) Pitch moment

Figure 5 Comparison between 70 SPs model and CFD results

3.2 Optimization Results of WBN Configuration

In this section, the deflection of flaps and ailerons were optimized at different lift and Mach number separately, with the object of minimum drag based on 57 SPs RSM models mentioned in above section.

The optimization results at cruise point, Ma=0.85, C_L=0.51 and three off-design points: Ma=0.85, C_L=0.48,0.55 and Ma=0.80, C_L=0.51 are listed in Table 1. At the cruise point, the maximum of drag reduction is 1.2 Counts with the pitch moment kept almost constant. At the off-design points, large profits of drag reduction can be obtained at Ma=0.85, C_L=0.55 and Ma=0.80, C_L=0.50, which are 5.1 Counts and 4.8 Counts, separately. The drag reduction at Ma=0.85, C_L=0.48 is much smaller than the other two off-design points, only 1.8 Counts. Figure 6 illustrates the pressure distribution of 6 span sections, which represent the local flow field at inner flap, KINK, outer flap, inner aileron, outer aileron and tip area. The lift and circulation distribution along span are shown in Figure 7. For both the cruise point and off-design points, the deflecting of flaps and ailerons mitigate the load of inner wing and enhance the load of outer wing, which makes the circulation distribution nearly elliptical, to reduce the induced drag further.

At the cruise point, the trailing edge deflecting didn't change the shock wave obviously except the outer aileron and tip area. The shock wave moves backward at this area and become a little stronger than that of the basic wing, as shown in Figure 6(a). Thus, it can be deduced the drag reduction at cruise point is mainly due to the induced drag reduction.

At the off-design point of cruise Mach number and higher lift (Ma=0.85, C_L=0.55), it can be seen in Figure 6(b) that the deflecting of flaps and ailerons weakens the shock wave at the area of outer flap and ailerons and changes its position. According to the pressure distribution, the reduction of wave drag can be concluded. Together with the induced drag described above, a large amount of drag reduction profit can be obtained after camber varied, and the drag should be decomposed to make clear which component contributes more.

At the off-design point of cruise Mach number and lower lift (Ma=0.85, C_L=0.48), no obvious change of shock wave is observed in Figure 6(c) except at the area of outer aileron and tip. The shock wave moves backward at this area without conspicuous change of intensity. The drag reduction is mainly due to the induced drag reduction.

For the last off-design point (Ma=0.8, C_L=0.51), the pressure distribution is quite different from the above conditions. The shock wave is formed near the leading edge. Therefore, the camber variation doesn't influence the shock wave effectively. It can be concluded that the reduction of induced drag dominates the considerable drag reduction profit.

Table 1 Deflection parameters and drag/pitch moment

	Inner flap	Outer flap	Inner aileron	Outer aileron	dC_D (Counts)	C_M
Ma=0.85, C_L=0.51	-1.0°	0.5°	0.5°	0.0°	-1.2	0.0004
Ma=0.85, C_L =0.55	0.1°	0.7°	1.1°	1.9°	-5.1	-0.019
Ma=0.85, C_L =0.48	-0.9°	0.1°	0.3°	0.7°	-1.8	-0.0021
Ma=0.80, C_L =0.51	0.2°	1.0°	1.7°	1.4°	-4.8	-0.022

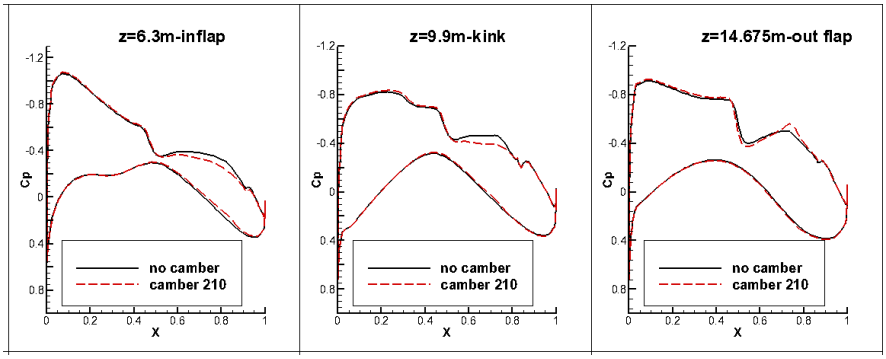

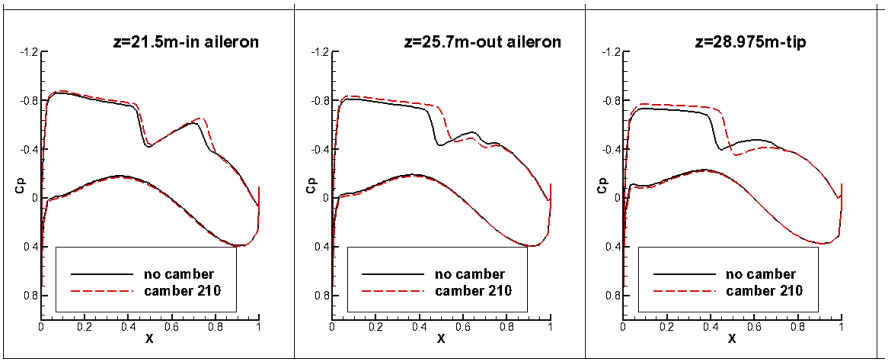

(a) Ma=0.85, C_L=0.51

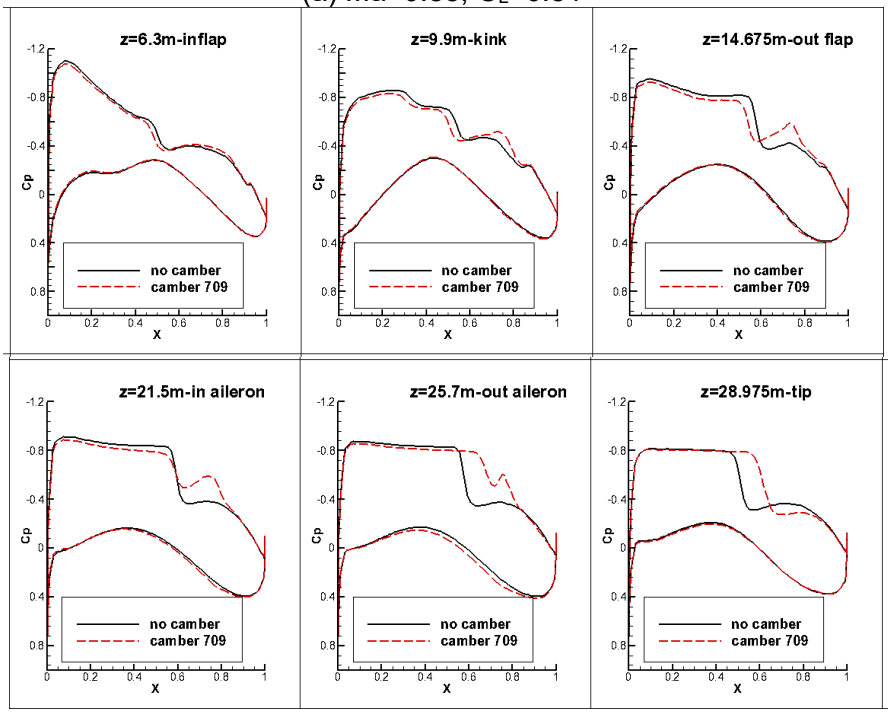

(b) Ma=0.85, C_L=0.55

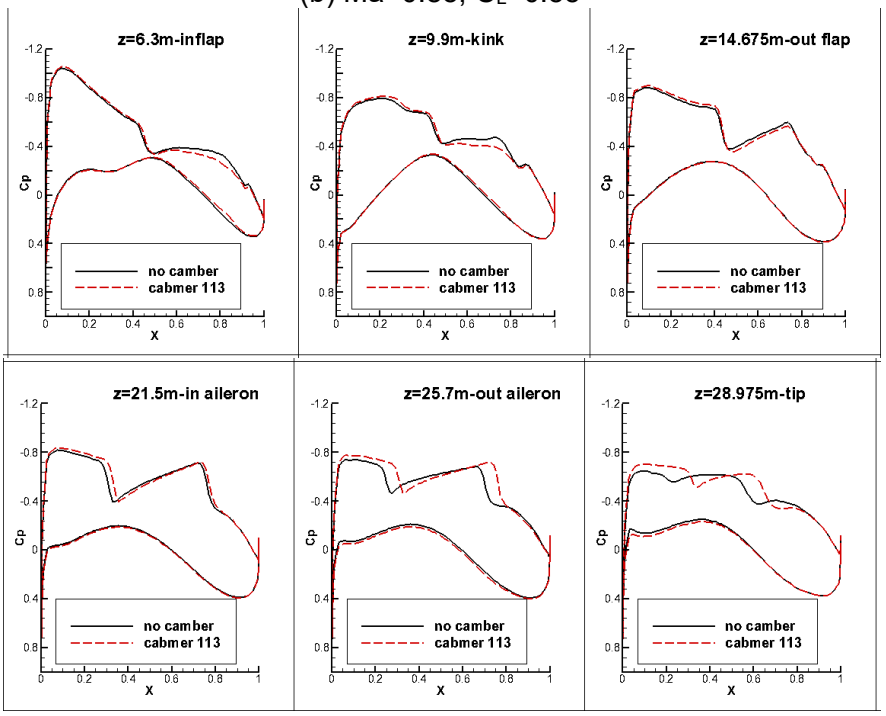

(c) Ma=0.85, C_L=0.48

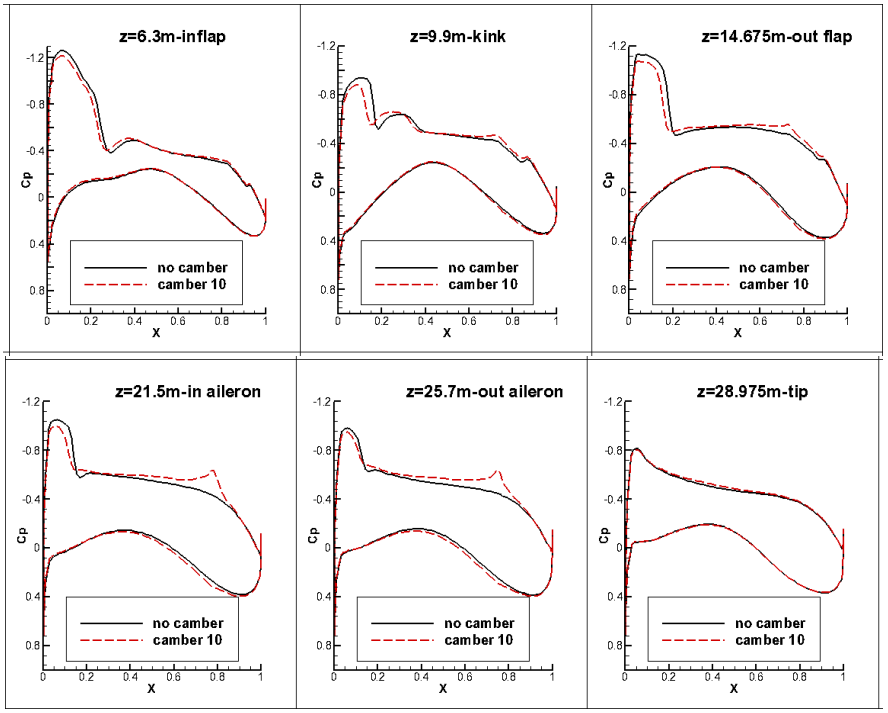

(d) Ma=0.80, C_L=0.51

Figure 6 Pressure distribution of WBNs

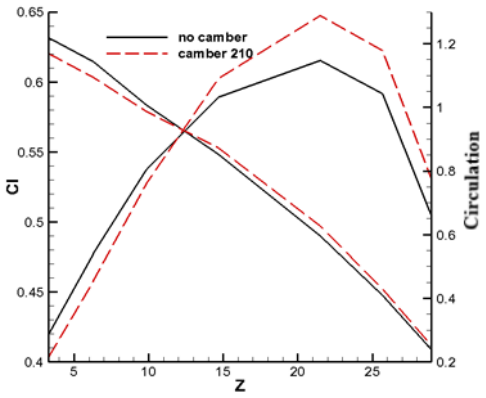

(a) Ma=0.85, C_L=0.51

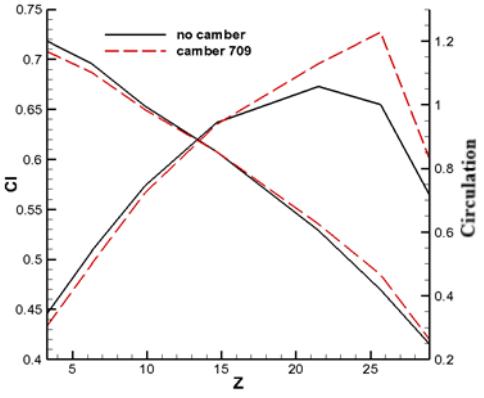

(b) Ma=0.85, C_L=0.55

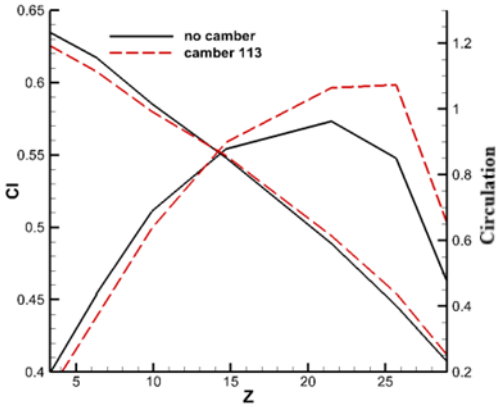

(c) Ma=0.85, C_L=0.48

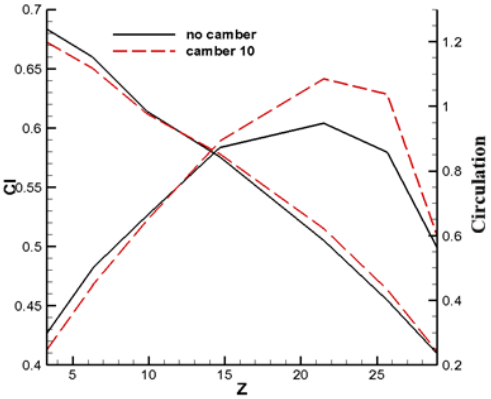

(d) Ma=0.80, C_L=0.51

Figure 7 Lift and circulation distribution of WBNs

3.3 Camber Influence on Trim Characteristics

In this section, the trimmed aerodynamic characteristics of the WBNT configurations with different camber variation settings at cruise point were analyzed based on CFD results to learn about the impact of camber variation on trim ability of horizontal tail. The WBNT configurations with different deflection of flaps and ailerons were trimmed by deflecting the elevator.

The drag increment and pitch moment of WBN and the drag increment of trimmed WBNT of the 6 camber variation settings are listed in Table 2. It can be seen that the WBN configuration from No. 2 to No. 5 can get a drag reduction of 0.5-0.7 Count accompanied by the pitch moment reduction of configuration No. 2 and No. 3. The spanwise pressure distribution of horizontal tail of the above-mentioned configurations are given in Figure 8. It can be seen that the deflection of the inner flap brings a considerable influence on the flow around the tail. The comparison of drag and pitch moment between WBNs and WBNTs without trimming are shown in Figure 9. For the configuration of No. 2, 3 and 4, the drag reduction of trimmed WBNTs is smaller than that of WBNs, which means these configurations have larger trim penalty of drag than the fixed camber configuration. While for configurations of No. 6 and No. 7, the smaller drag increment of trimmed WBNT means the two configurations have smaller trim penalty of drag than the fixed camber configuration. A more divergent discrepancy of pitch moment can be observed, but same conclusion about trim penalty can be obtained. Besides the drag and pitch moment, the lift coefficients of horizontal tail of trimmed WBNTs are also different, varying from -0.033 to -0.035. The quite different discrepancy of drag and pitch moment between WBN and trimmed configuration implies the changed trim ability of horizontal tail due to camber variation.

The horizontal tails' lift and pitch moment of untrimmed WBNT configurations with different inner flap deflection are illustrated in Figure 10. It can be seen that the lift of horizontal tails is proportioned to the deflection angle of inner flap and the pitch moment has a nearly linear relation with the deflection angle of inner flap. It can also be found that a nearly linear variation of pitch moment of No. 4-7 WBNT configurations with an increment 0.2 of inner flap deflection and same deflection of outer flap, although the pitch moment for WBNs are quite divergent. For this model, the half span of the horizontal tail and KINK are 9.4m and 9.9m, separately. Thus, based on the above-mentioned results, it can be concluded that compared with the pitch moment, the camber variation of inner wing caused by inner flap deflecting dominates the influence on trim penalty. Although the pitch moment of No. 2 WBN configuration decreases, the upward deflecting of inner flap weakens the downwash of the wake, which decreases the equivalent incident angle of the wake flow. Thus, the trim ability of horizontal tail becomes worse, which results in more trim penalty of drag. On the contrary, a comparable drag reduction but much higher pitch moment of No. 5 WBN configuration can still get drag reduction after being trimmed with a tiny trim penalty of drag. Therefore, the upward deflection of inner flap should be restrained to ensure the solution favorable to trim when nose-down moment exists.

Table 2 Deflection parameters and drag/pitch moment

	Inner flap	Outer flap	Inner aileron	Outer aileron	dC_D_WBN (Counts)	dC_M WBN	dC_D_trim (Counts)
1	0	0	0	0	0	-	0
2	-1.2	0.7	0.4	-0.2	-0.7	0.0015	1.1
3	-0.6	0.2	0.7	-0.4	-0.6	0.0015	0.1
4	-0.2	0.2	0.4	0.32	-0.5	-0.0035	0.1
5	0	0.2	0.3	0.2	-0.5	-0.02868	-0.4
6	0.2	0.2	0.3	-0.2	0.2	-0.0038	-0.0
7	0.4	0.2	0.3	-0.2	0.8	-0.0053	0.3

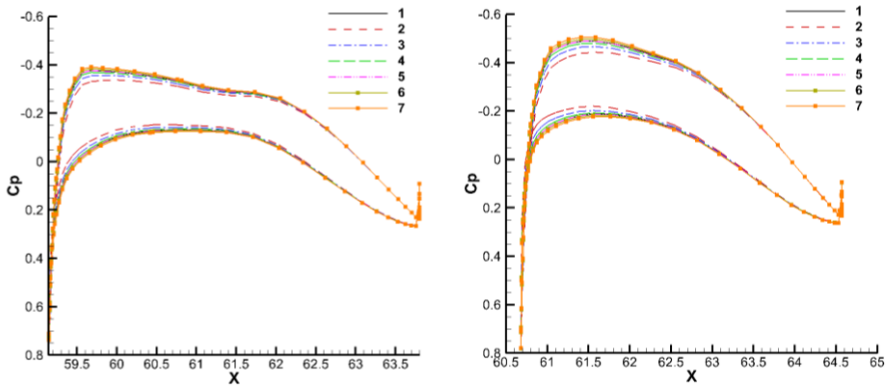

(a) Z=3m (b) Z=5m

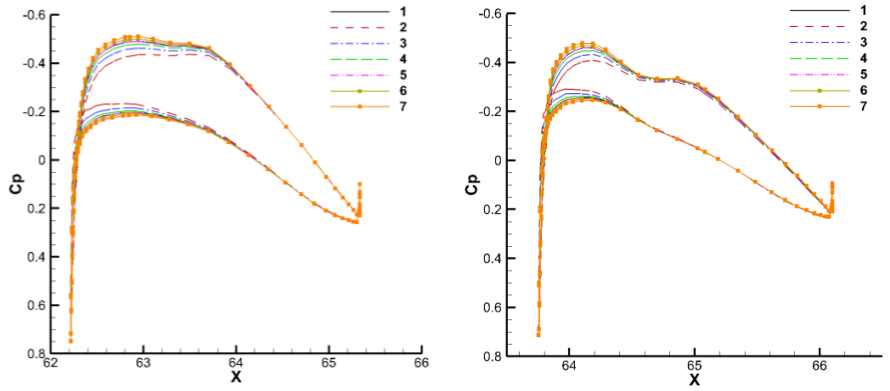

(c) Z=7m (d) Z=9m

Figure 8 Pressure distribution of horizontal tail of WBNT without trimming

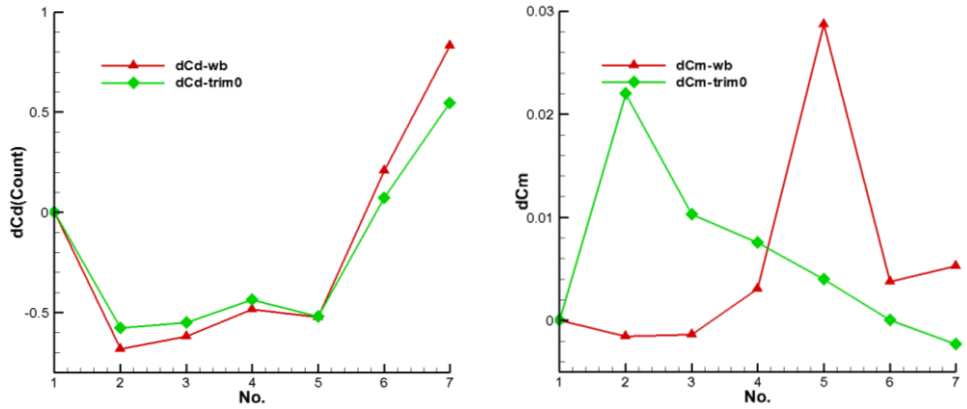

Figure 9 The increment of drag and pitch moment of WBN and WBNT without trimming.

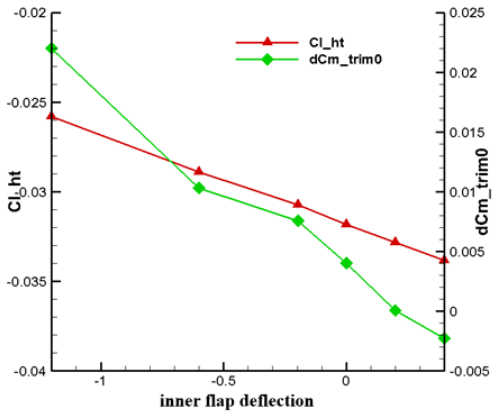

Figure 10 lift and pitch moment of WBNT Horizontal tail without trimming

3.4 Drag Characteristics of Trimmed WBNTs

The optimal results and some preferable results during optimization were selected to compare the trimmed drag characteristics to obtain the final camber variation settings. The maximum drag reduction at cruise point, Ma=0.85, C_L=0.48 and three off-design points, Ma=0.85, C_L=0.45, 0.52 and Ma=0.80, C_L=0.48 are listed in Table 3. It can be seen that the camber variation settings for maximum drag reduction of trimmed WBNTs are quite different from the WBNs. Figure 11 illustrates the pressure distribution of WBNTs at 6 span sections. The lift and circulation distribution along span are shown in Figure 12. The similar variation of load distribution can be found in Figure 7 and Figure 12 despite the different deflection of flaps and ailerons. At all of the four optimization points, the camber variation of wing improve the circulation distribution and the induced drag are decreased.

At the cruise point, the slight deflecting of outer flap and ailerons makes a very tiny change of shock wave. Only the shock wave at the tip area moving backward inconspicuously can be observed in Figure 11(a). The drag reduction at cruise point is almost from the induced drag reduction.

For the off-design points at cruise Mach number and higher lift (Ma=0.85, C_L=0.52), it can be seen in Figure 11 (b) that the pressure distribution is quite similar with the WBN configuration except the area of ailerons. The deflecting of flaps and ailerons doesn't weaken the shock wave as much as that of WBN configuration. Although this camber variation is not the best setting for WBN configuration, the larger downward deflection of inner flap brings a profit to the horizontal tail for trimming, which gains the maximum drag reduction for trimmed WBNT configuration.

For the off-design points at cruise Mach number and lower lift (Ma=0.85, C_L=0.45), the pressure distribution in Figure 11 (c) is quite similar with that of the WBN. The shock wave at the area of outer aileron and tip section moves backward with inconspicuous change of intensity. The drag reduction is mainly due to the induced drag reduction. For this condition, the upward deflecting of inner flap doesn't result in an obvious trim penalty of drag. At lower lift, the WBNT configuration is in over-trimmed condition, the upward deflecting of inner flap weakens the downwash of wake, which is favorable for trimming.

For the last off-design point (Ma=0.8, C_L=0.48), the deflection parameters of WBNT configuration is the same as the WBN configuration. The shock wave appears near the leading edge, thus it is hard to influence the shock wave for trailing edge camber variation The reduction of induced drag dominates the considerable drag profit.

Table 3 Deflection parameters and drag reduction of trimmed WBNTs

	Inner flap	Outer flap	Inner aileron	Outer aileron	dC_D (Counts)
Ma=0.85, C_L=0.48	0	0.2	0.3	0.2	-0.4
Ma=0.85, C_L=0.52	0.4	0.8	1	2	-3.0
Ma=0.85, C_L=0.45	-0.6	-0.3	0.4	0.7	-0.9
Ma=0.80, C_L=0.48	0.2	1.0	1.7	1.4	-2.0

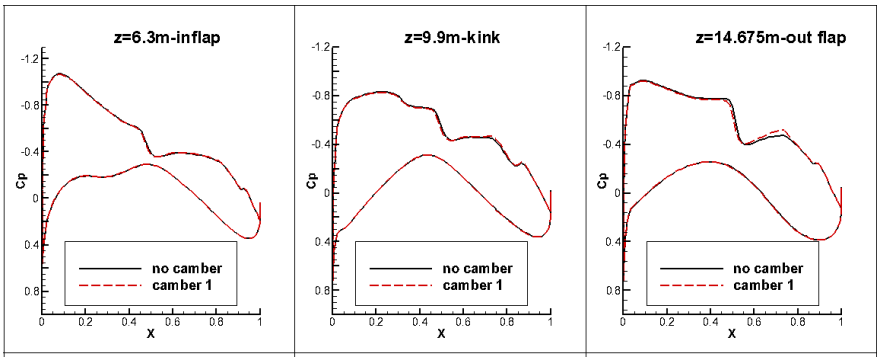

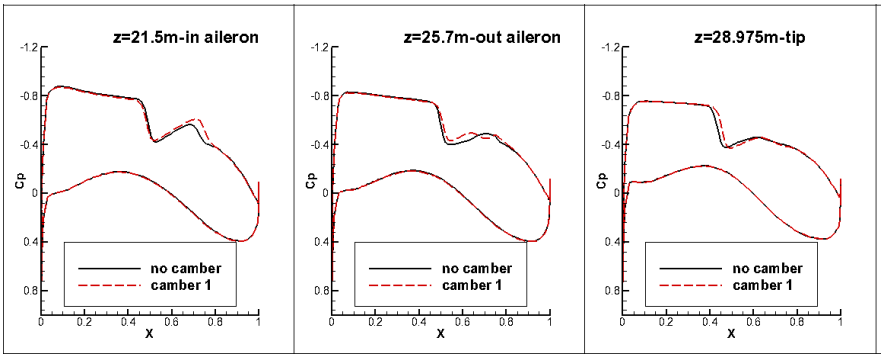

(a) Ma=0.85, C_L=0.48

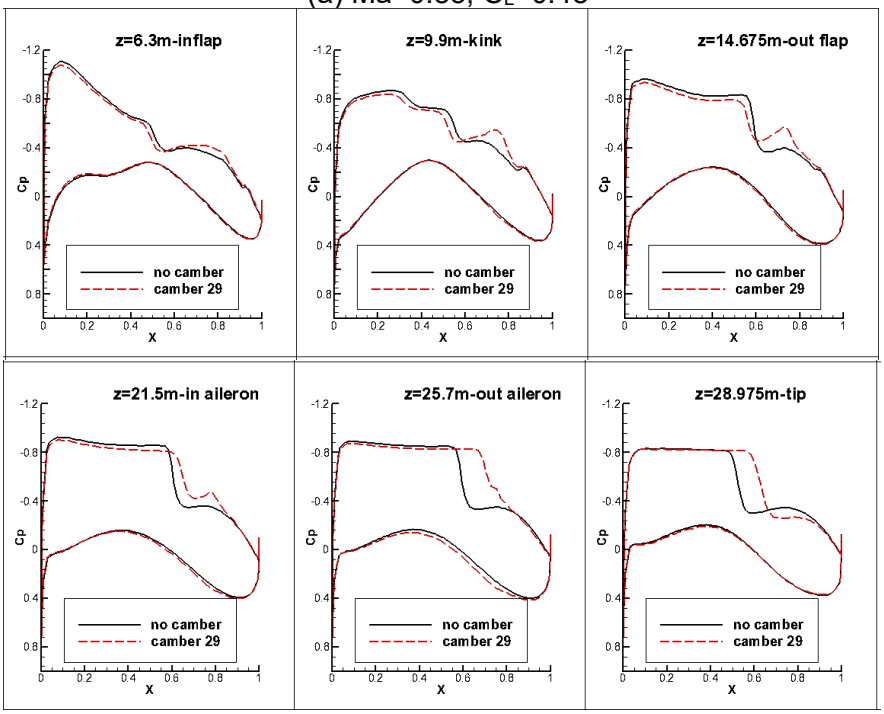

(b) Ma=0.85, C_L=0.52

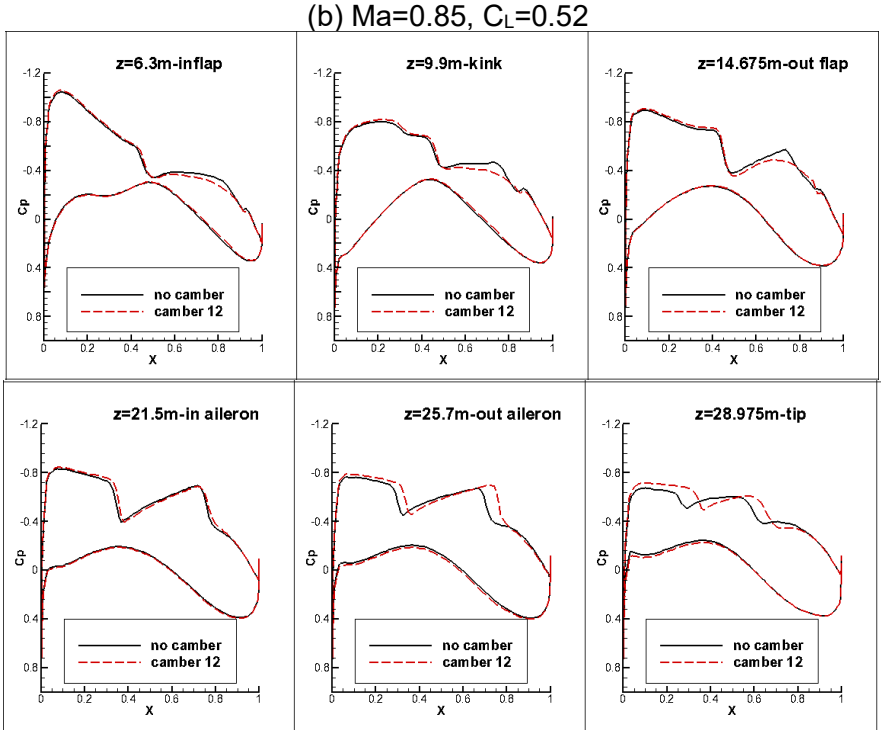

(c) Ma=0.85, C_L=0.45

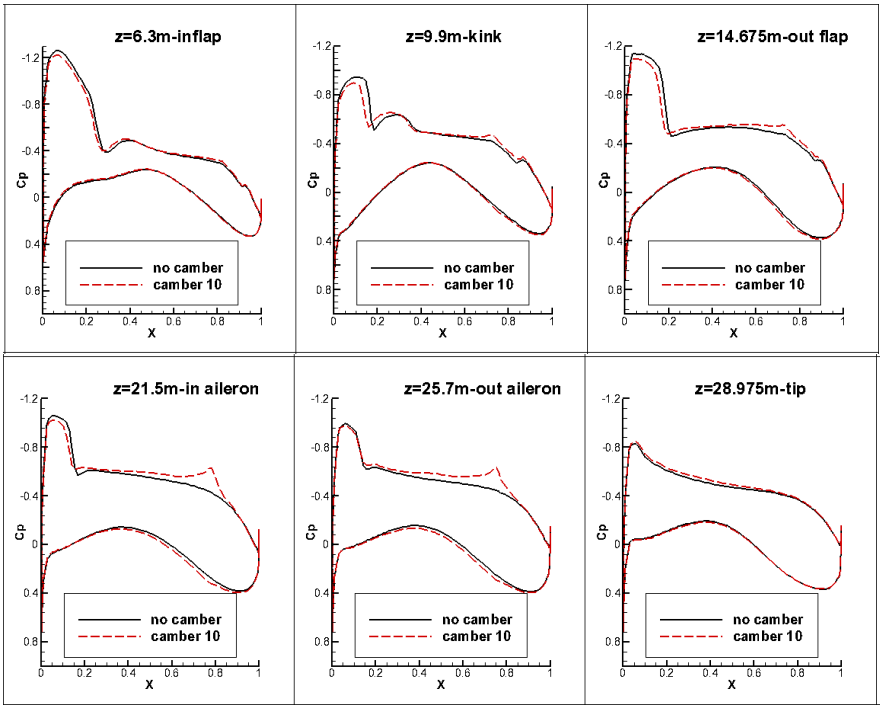

(d) Ma=0.80, C_L=0.48

Figure 11 Pressure distribution of trimmed WBNTs

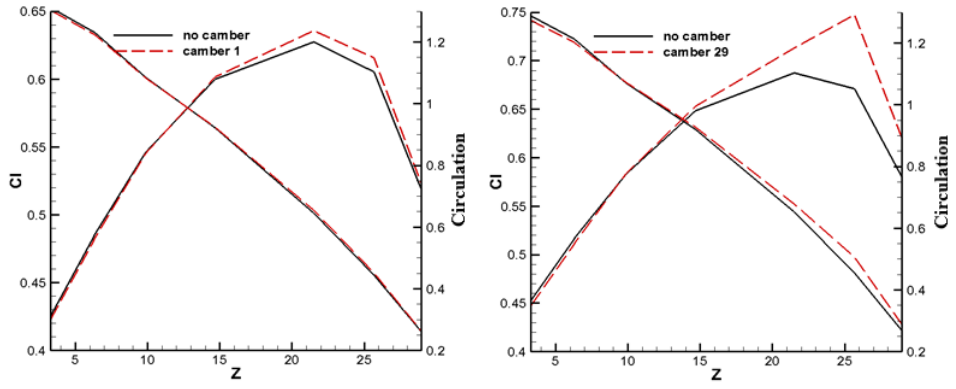

(a) Ma=0.85, C_L=0.48 (b) Ma=0.85, C_L=0.52

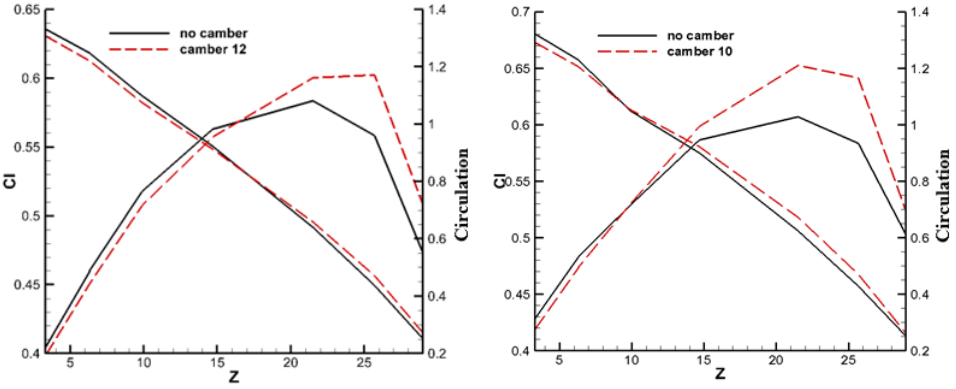

(c) Ma=0.85, C_L=0.45 (d) Ma=0.80, C_L=0.48

Figure 12 Lift and circulation distribution of WBNs

4. Conclusion

In this paper, the drag reduction of wide-body transport were researched by varying the camber of wing through deflecting the flaps, ailerons and spoilers. The deflection of flaps and ailerons of WBN configurations were optimized based on Genetic algorithm. The accurate response surface

models based on high fidelity CFD results were developed to realize the fast prediction of aerodynamic characteristics. The multi-step optimization was carried out to research the necessary number of sample points for the RSM model that can predict the drag precisely. The two-step optimization and about 60 sample points can ensure an accurate model in this paper.

The deflection angle of flaps and ailerons of WBN configurations were optimized at designed cruise point and 3 off-design points. The drag can be reduced at all of the four flight conditions with varying the camber of wing, and the amount is about 1-5 Counts from both the induced drag and wave drag reduction. The higher the lift is, the more drag reduction can be obtained.

The trim characteristics of the variable camber wing configurations were researched. The deflection of inner flap changes the downwash of the wake, which impose an obvious influence on the flow around the tail and the trim ability of the horizontal tail is changed. Thus, for the higher lift cases that the obvious nose-down moment would generate, the upward deflection of inner flap should be restricted to avoid a large amount of trim penalty of drag. Based on the above analysis, the optimization of the variable camber wing based on the trimmed configuration would be better and more feasible, which will be carried out in the future.

5. Copyright Statement

References

[1] Gilyard G., Martín España, On the use of controls for subsonic transport performance improvement: overview and future directions, NASA TM-4605, 1994.

[2] Gilyard G. B., Georgie J, Barnicki J. S., Flight test of an adaptive configuration optimization system for transport aircraft, NASA TM-1999-206569 1999.

[3] Szodruch J. Hilbig R., Variable wing camber for transport aircraft, *Prog. Aerospace Sci.*, Vol. 25, pp.297-328,1988,.

[4] Szodruch J., The influence of camber variation on the aerodynamics of civil transport aircraft, AIAA Paper 85-0353, 1985.

[5] Hilbig R., and Wagner H., Variable wing camber for civil transport aircraft, ICAS Paper 185-5.2.1, 1984.

[6] Greff D. E., Aerodynamic design and integration of a variable camber wing for a new generation long/medium range aircraft, ICAS Paper 88-2.2.3, 1988.

[7] Boeing Commercial Aircraft Company, Assessment of Variable Camber for Application to Transport Aircraft, NASA CR-158930, 1981.

[8] Roe, P. L., Approximate Riemann Solvers, Parameter Vectors, and Difference Schemes, *Journal of Computational Physics*, Vol. 43, pp. 357–372, 1981.

[9] Menter F. R. Zonal two-equation k-ω turbulence model for aerodynamic flows, AIAA Paper 93-2906, 1993.

[10] Guo Shaojie, Zhou Peipei, Wang Bin, Shi Xiaotian. Numerical Investigation for influence of powered effect on aerodynamic characteristics of civil aircraft take-off configuration,. *Journal of Aerospace Power*, Vol. 31, No. 7, pp. 1638-1648, 2016.

[11] Guo Shaojie, Wang Bin, Su Cheng. et al. Numerical simulation for the effect of engine failure on longitudinal aerodynamic characteristics of a civil aircraft take-off configuration. *Advances in Aeronautical Science and Engineering*, Vol. 7, No. 2, pp. 143-151, 2016.

[12] Goldberg D. E., “Genetic Algorithms in Search, Optimization and Machine Learning,” Addison-Wesley, Reading, MA, 1989.

[13] M. Papila, R.T. Haftka, Response surface approximations: Noise, error repair, and modeling errors, AIAA Journal, Vol. 38, No. 12, pp. 2336–2343, 2000.

[14]Helton, J.C. and F.J. Davis. "Latin Hypercube Sampling and the Propagation of Uncertainty in Analyses of Complex Systems," Reliability Engineering and System Safety, Vol. 81, No.1, pp. 23-69, 2003.